We are IntechOpen, the world's leading publisher of Open Access books Built by scientists, for scientists

6,900
Open access books available

185,000
International authors and editors

200M
Downloads

Our authors are among the

154
Countries delivered to

TOP 1%
most cited scientists

12.2%
Contributors from top 500 universities



WEB OF SCIENCE™

Selection of our books indexed in the Book Citation Index in Web of Science™ Core Collection (BKCI)

Interested in publishing with us?
Contact book.department@intechopen.com

Numbers displayed above are based on latest data collected.
For more information visit www.intechopen.com



Chapter

Taxonomy of Big Nuclear Fusion Chambers Provided by Means of Nanosecond Neutron Pulses

Vladimir Gribkov, Barbara Bienkowska, Slawomir Jednorog, Marian Paduch and Krzysztof Tomaszewski

Abstract

A methodology is elaborated and applied to taxonomy of large chambers of thermonuclear fusion reactors. It ensures a feasibility to describe impairments produced by environment and details of the chamber into the neutron field generated during the operation of a reactor. The method is based on application of very bright nanosecond neutron flashes irradiated from a compact neutron source of a dense plasma focus type. A number of neutron activation procedures as well as a neutron time-of-flight method were applied to trace deviations of neutron 3-D fields after their interaction with the simulator of the above chamber. Monte-Carlo modeling of these processes gained the data on the most important elements that influenced on the fields.

Keywords: nuclear fusion reactors, dense plasma focus, nanosecond neutron pulses, neutron activation diagnostics, time-of-flight spectral diagnostic

1. Introduction

Contemporary and future nuclear fusion reactors are of rather sophisticated assemblies positioned in intricate surroundings. Elements of their environment and constructions may absorb and scatter the basic fusion energy carriers—neutrons [1].

The contemporary main-stream nuclear fusion installations using magnetic and inertial plasma confinement, namely: Joint European Torus (JET, U.K.) [2], Wendelstein 7X Stellarator (W7X, Germany) [3] (in the nearest future—the International Thermonuclear Experimental Reactor (ITER) [4]), the powerful laser devices Iskra-5 (in future Iskra-6, R.F.) and National Ignition Facility (NIF, U.S.A.) [5] as well as the Z-Machine [6] (Jupiter expected in future [7], U.S.A.)—generate around their chambers 3-D neutron fields that are distorted at their irradiation outside. The elements of the sheds, numerous structures of the Nuclear Fusion Chambers (NFC), power sources as well as specific apparatus belonging to these parts of the facilities exemplify scatterers and absorbers irradiated by neutrons. So produced by the fluctuations ("voids" and "hot spots") in neutron intensity and in spectra around the NFC must be taken into account at the interpretation of the operational results. The neutron intensity changes and spectra imperfections observed out of NFC because of elastic and inelastic neutron scattering may happen

even at an absolutely isotropic initial expansion of neutrons into space from a source with symmetric nuclear fusion neutron spectral content (e.g., from a laser target in a laser fusion facility or from an element of the toroidal plasma ring in a tokamak).

But there is an opportunity to describe a 3-D neutron field formed around a nuclear fusion chamber before its full-scale operation with a help of a foreign powerful point neutron source that has pulse duration in a nanosecond (ns) range. Indeed the intense short neutron flash will allow attributing and describing all elements of a NFC that absorb and/or scatter neutrons separately by using measurements of neutron fluxes (with neutron activation methods) and spectra (with photomultiplier tube plus plastic scintillator—PMT + S—by means of time-of-flight (TOF) method) in all directions. These two procedures will also be important from the point of view of the radiation material science: they will give information where one may expect increased or diminished values of *dpa* in the plasma-facing and construction materials of a NFC.

A very intense ns neutron pulse irradiated from a tiny volume (about 1 cm^3) can be generated by a nuclear fusion device named dense plasma focus (DPF) [8]. Moreover, its neutron emission is quasi-mono-energetic one. So by means of this device, one may have an opportunity to distinguish elastic scatterings produced by different parts of a chamber or by dissimilar chemical elements of their content. DPF may also be used in time-of-flight technique for spectra measurements with a moderate path length.

Nuclear fusion reactions in a DPF are produced at the interaction of self-generated and magnetized fast deuterons with pinched plasma [8]. It is similar to the process taking place in tokamaks with an external neutral beam heating of its plasma. Accelerated fast deuterons have spectrum spreading to MeV range and peaked at hundreds keV. The DPF device may be exploited with *D* or *D-T* mixture as working gases. In these cases, it will produce neutrons with mean energy at around 2.5- or 14-MeV energy peaks correspondingly as it is so in the contemporary main-stream NFCs. With these ns neutron pulses, a majority of materials used in activation technique will have the activation time much shorter compared with the time of their radioactive decay.

Nanosecond neutron pulses are irradiated from the DPF chamber into space as a neutron "shell" (**Figure 1a**) of a finite thickness. It has almost a spherical shape. The thickness of the shell (i.e., a space between the surfaces *A* and *B* of the sheath filled

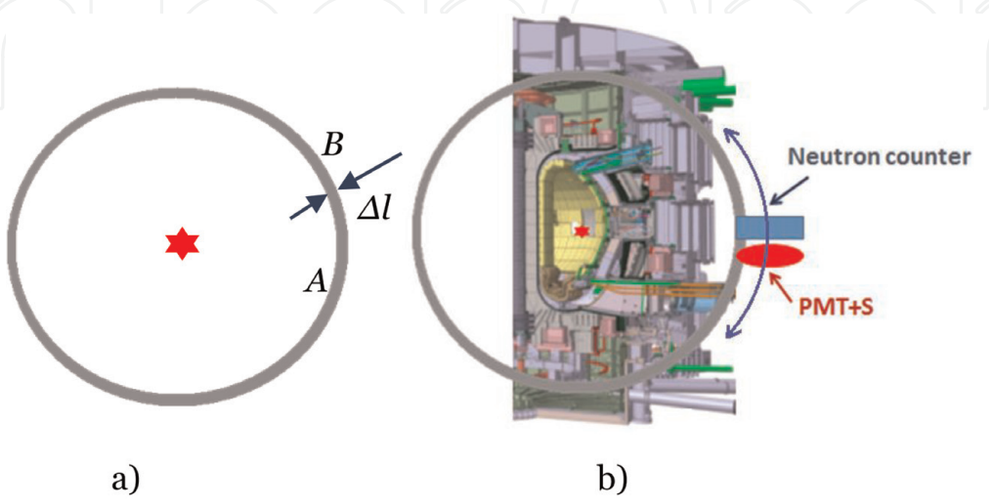


Figure 1.
A neutron "sheath" (a) irradiated from a compact neutron source (shown by a star) of an ns pulse duration having a thickness in space Δl given by formula (1); its possible use (b) in a large main-stream NFC (a sketch of a cross-section of the ITER chamber is here).

with neutrons) has a value Δl equal to pulse duration of neutron radiation Δt multiplied by neutron speed v:

$$\Delta l = \Delta t \times v \tag{1}$$

This sheath during its propagation from the compact source outwards will be distorted because of absorption and scattering on elements and systems belonging to a NFC. Thus, such a source can be able to uncover each element of a NFC producing the above-mentioned distortions during neutron radiation expansion through the chamber components (**Figure 1b**).

These alterations may be found in data on the absolute neutron flux measured in certain 3-D points in the exterior of the chamber. It will also be discovered as confident modifications in a neutron temporal evolution in time and, consequently, in neutron spectral composition after their transit through elements and systems of the nuclear reactor.

The spatial thickness of the above neutron "shell" will have a value of about 10 of cm being much less compared with the main construction elements of a NFC of a main-stream fusion facility. Thus, for the taxonomy of objects by such a bright

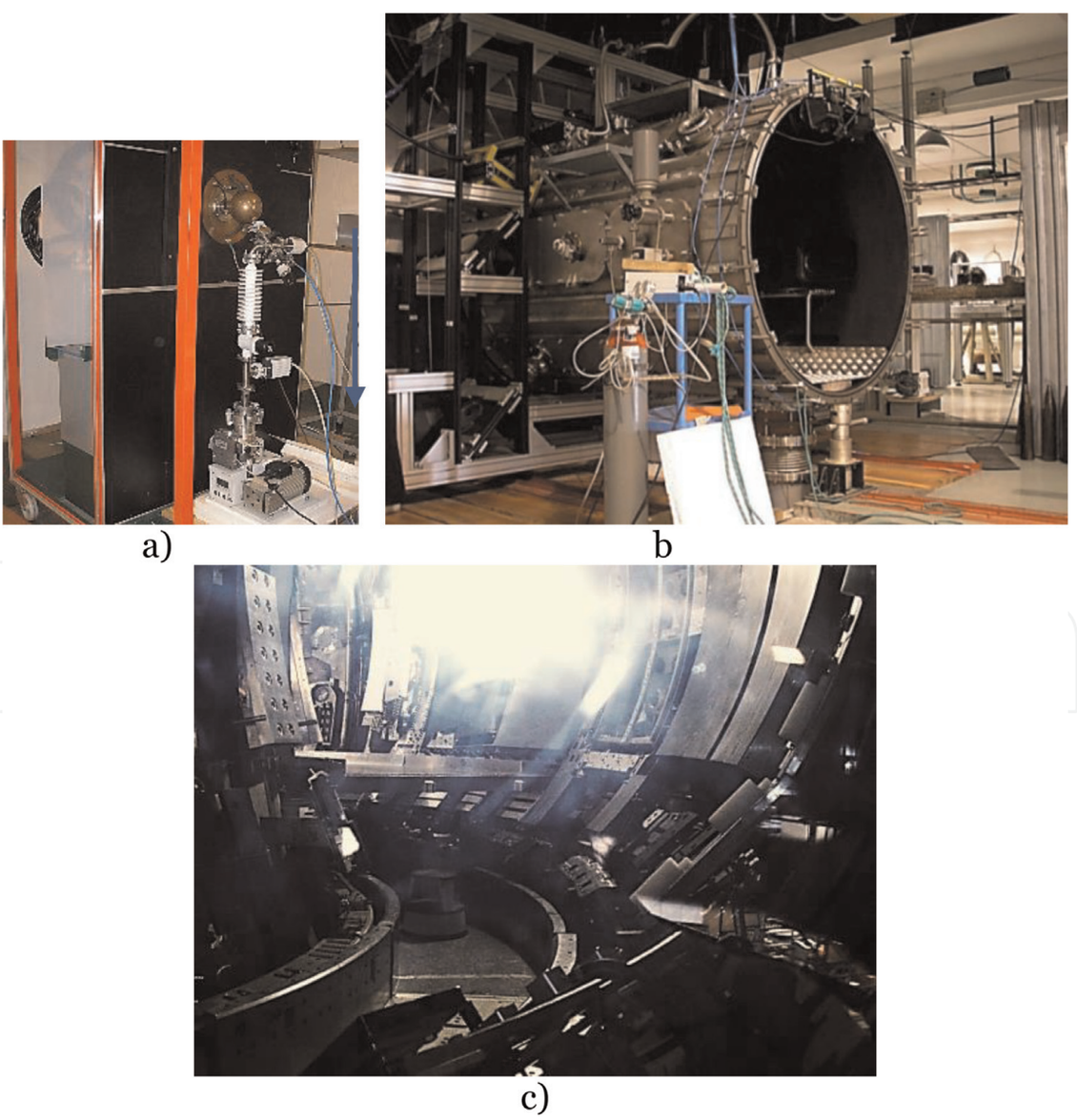


Figure 2.
Dense plasma focus device PF-6 (a) and a big chamber of the PF-1000U facility (b), simulating a section of a main-stream fusion chamber of a present-day tokamak (JET here) (c).

short-pulse neutron radiation, one may use elastic and inelastic scattering of neutrons upon nuclei of unknown elements. It is evident that this short powerful neutron flash allows using TOF technique with short flight bases for modern NFCs.

This type of measurements can be provided by positioning of a DPF-based compact neutron source in the center of the spherical chamber used in laser fusion facility or at the movement of this neutron source along the circumference of the toroidal chamber of a modern fusion device with magnetic plasma confinement. Such characterization procedures should preferably be repeated after each important stage of assembling of a new main-stream fusion facility to describe its novel elements and their influence on neutron field.

Here in the very beginning, we shall observe the activation methods applied by using ns neutron pulses generated in a DPF device PF-6 (**Figure 2a**) due to *D-D* reactions. Thus, the generated in the device 2.5-MeV neutrons are subjected mainly to elastic scattering on parts and structures of a simulator of a NFC [1]. Then later, a neutron spectroscopic technique will be talked over.

In this case, we exploit in the capacity of the simulator of a big NFC a large chamber that belongs to the PF-1000U facility [9] available at the Institute of Plasma Physics and Laser Microfusion (**Figure 2b**), Poland. This chamber looks quite similar to the section of JET tokamak (U.K.)—**Figure 2c**. The vacuum chamber of the PF-1000U device has a shape of a large cylinder with walls made of stainless steel. The discharge circuit of the chamber consists of a set of capacitors, cables, and spark-gaps connecting the battery with cylindrical concentric electrodes playing the role of a plasma accelerator.

2. The PF-6 device as a compact ns-pulsed neutron source and its auxiliary facilities

2.1 PF-6 device

This machine (**Figure 2a**) has been described in a number of papers (see e.g., [1, 10–12]). Its battery charged to 12–20 kV contains up to 6 kJ of energy. Typical range of initial pressures of pure deuterium in the device in this configuration was in the range from 2 to 8 Torr. Amplitude of a discharge current of the device measured by a Rogowski coil reaches 0.7 MA. The definition of the device as a neutron source (its major parameters that were measured many times) is as follows:

- Neutron emitting plasma volume is less than 1 cm^3; so it is much smaller compared with a several-meter characteristic size of a main-stream NFC elements and systems; thus it may be counted as a point very bright mono-energetic source.

- Quasi-mono-energetic spectra of neutrons are different to some extent being measured at dissimilar angles to Z-axis of the device; they are peaked near the energy about 2.5 MeV with the narrow spectrum near it: $\Delta E_n/E_0 \approx 3$–5%, where ΔE_n—full width of neutron energy distribution function at its half maximum (FWHM), and E_0 is an energy value where the peak of neutron energy distribution is observed in a particular direction.

- Neutron yield is 10^8–10^9 neutrons/pulse with the deuterium chamber filling and about two orders of magnitude higher for the *D-T* mixture as a working gas.

- Pulse duration is in the range 15–20 ns, that is, a "thickness" of a quasi-spherical neutron "sheath" (**Figure 1a**) spreading into a space from the source has its value of about 10 cm. In other words, 10 cm is the length of the neutron packet coming to a detector from the neutron source. Thus, the DPF source irradiates an ns neutron pulse to a detector as a neutron bunch with a size much smaller than the characteristic dimensions of the elements and systems of a NFC.

A DPF is an ecologically more acceptable radiation-producing device in comparison with another neutron sources like the accelerators, fission reactors, and isotope-based sources because:

- Its battery charging voltage is relatively low (~10 kV).

- The DPF is a so-called "push-button source" because it irradiates neutrons during several nanoseconds merely at switching it on.

- It does not demand safe containers for the device's protection.

- This set-up can be supplied with a sealed chamber having a *D-T* gas mixture generator with a heater discharging the gas into the chamber's volume [13].

In **Figure 3**, the oscilloscope trace of the current derivative of a typical "shot" (discharge) of the device is presented. Chambers that have been used in this device were of two types (small and large) designed and manufactured at the VNIIA. With the last one, it may be sealed, obeying a gas generator with deuterium-tritium mixture and produce the 14-MeV neutrons with the yield up to 10^{11} neutrons of 15–20 ns time duration.

2.2 Activation methodology

A silver activation counter—SAC [1] (in fact two of them—SAC-1 and SAC-2) is the main tool in this technique of measurements of the absolute neutron yield Y_n. It is based on silver as activated material. The whole detector is composed of a Geiger-Muller (G-M) counter wrapped with a silver foil and placed within a hydrogen-reach moderator. Fast neutrons (2.5 MeV) emitted from a DPF source are slowed

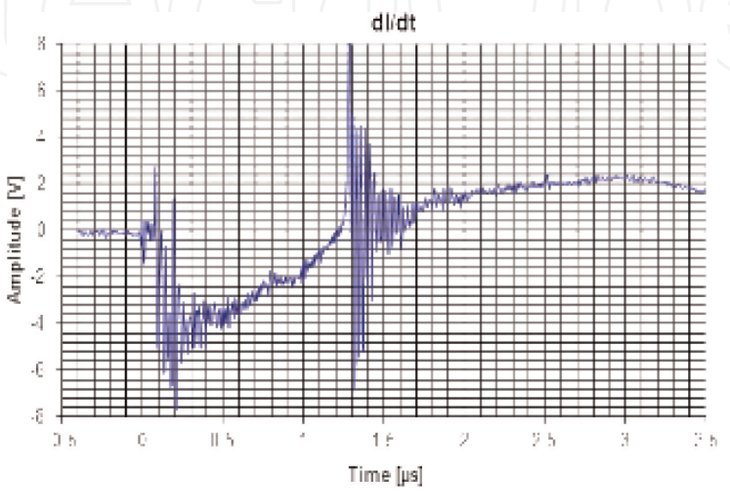


Figure 3.
Oscillogram of the current derivative for a typical "shot" of the PF-6 device.

down in the moderator. Indirect products of two reactions of decelerated neutrons with *Ag* are β^- emitters. This type of neutron detectors is a wide-spread tool in the DPF community, in particular because of the short (ns) neutron pulses generated by a DPF that is much shorter compared with the half-life of the reactions (see **Table 1**). We used these detectors with and without cadmium foil enveloping our moderators of SACs. With this foil, the effective "threshold" of neutrons' energy registered by the counter is 500 keV. In this case, slow neutrons coming to the detector after scattering in the surroundings are not registered. SACs that were used since many years as the Y_n monitor for the PF-6 device were calibrated many times by special isotope-based neutron sources placed inside the device's chamber. The calibration of SACs has been combined with MCNP calculation [14].

The SAC method has a number of limitations. It can be better operational if it will be used in a combination with other methods of Y_n monitoring. So other elements [14–18] (*In*, *Be*, and *Y*) were exploited for a so-called cross-calibration technique with SACs. In a **Table 1**, one may see the most important nuclear data regarding the nuclear reactions that were engaged in the PF-6 neutron activation monitors. Here, $T_{1/2}$ is the half-life time of particular radionuclides.

The elements have been chosen because of their specific advantages. Thus, a cross-section for the reaction with *Be* (the BNAC detector) has an effective threshold near 1 MeV, so undesirable multiple-scattered neutrons do not undergo this reaction and, therefore, are not measured. The inelastic scattering reaction with *In* has such a threshold equal to 340 keV. Fusion neutron yttrium monitor (FNYM) does not need any neutron moderator to allow neutrons detection.

A large area gas sealed proportional detector SP-126C (Canberra made) has been chosen in these techniques as a β^- particle counter. Its calibration includes the following procedures: use of calibration sources of β^- and neutron radiations with a parallel set of various Monte Carlo calculations for β^- particle and neutron transport. We applied the MCNP5 [16] Monte Carlo code with MCNP5DATA [17] cross section library that have been used for the above-mentioned calculations.

In some of the above-mentioned activation techniques, the gamma spectrometry system based on the high purity germanium (HPGe) detector equipped with multichannel analyzer (MCA) was used. The detector is supplied by the

Irradiated element	Nuclear reaction	Reaction's product	Half-life decay, $T_{1/2}$[a]	Mean energy E_β (keV)	Intensity (%)
^{107}Ag [14]	n,γ	^{108}Ag	2.382 m	629	95.5
^{109}Ag [14]	n,γ	^{110}Ag	24.56 s	1199.36	95.18
^{9}Be [14–18]	n,α	^{6}He	806.7 ms	1567.62	100
				E_γ (keV)	Intensity (%)
^{115}In [14]	n,n′	^{115m} In	4.486 h	336.241	45.8
^{115}In [14]	n,γ	^{116}In	54.29 m	1293.56	84.8
				1097.28	58.5
				416.90	27.2
				2112.29	15.09
^{89}Y [14]	n,n′	^{89m} Y	15.663 s	908.960	99.16

[a] *http://www.nndc.bnl.gov/nudat2/dec search.jsp.*

Table 1.
Nuclear data relating to the nuclear reactions that are engaged in neutron activation techniques.

manufacturer with its numerical characterization and software for mathematical calibration of the system (ISOCS/LABSOCS). Specific features of the above-mentioned activation methods, calibration procedures, and their MCNP support calculations one may find in the work [18].

2.3 Neutron spectroscopy based on the time-of-flight measurements

Time-of-flight (TOF) methodology was applied for the neutron spectra investigations with and without the above-mentioned simulator of a NFC. For this goal, two mobile measuring stands for experiments prepared to work in a harsh electromagnetic environment are used [1, 22]. The base for each measuring stand is the cabinet, which represent a Faraday cage featuring outstanding electromagnetic compatibility (EMC) shielding (it is possessed of 80 dB in the range from 30 to 300 MHz, of 60 dB in the range from 300 MHz to 1 GHz and up to 40 dB for the frequency band centered around 3 GHz).

At the data acquisition procedure, the stand is linked with the detectors and triggers only by the fiber optic connections (i.e., for triggering, time marking, and data transmission) with the devices positioned out of the stand, thus having no any galvanic contacts with the main lines and the experimental facilities. The stands are equipped with the converters for two-way signal conversion (**Figure 4**) and they are battery-powered.

The hybrid module is equipped with the photomultiplier tube (PMT) having 12 focusing dynodes. The conversion of ionizing radiation into light occurs in the fast organic scintillators S (so on the whole the system is named as a PMT + S—**Figure 5**).

Usually, the scintillators used in the device have 45 mm in a diameter and 50 mm of their length. This length was chosen due to its closeness to the mean free path of 2.5-MeV neutrons in it.

All PMT + Ss (these detectors will be named subsequently as TOF-1 or TOF-2) are inserted into the cylinders made of paraffin (served as collimators) and have a 2-mm lead foil blocking front part of the PMT + Ss to prevent them from scattered neutrons and soft X-rays. The oscilloscopes are triggered through the fiber optic cables. In **Figure 6**, one may see two stands near the PF-6 with the open door showing PMT + S, an oscilloscope and SACs on their roofs.

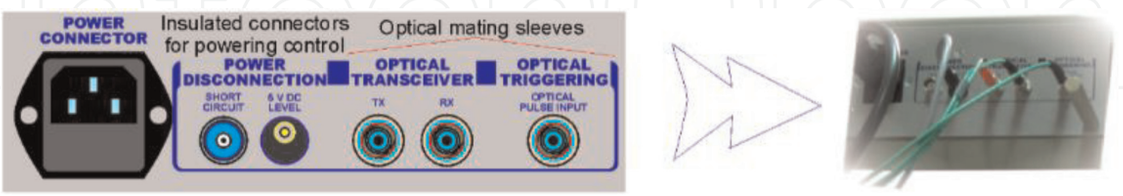


Figure 4.
Elements of mobile measuring stands used for powering management and optical communication [19].

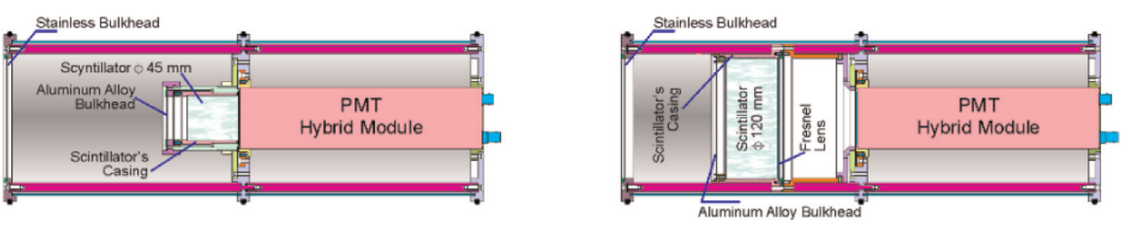


Figure 5.
Key components of the fast neutron scintillation probes (FNSP-1) [19]).

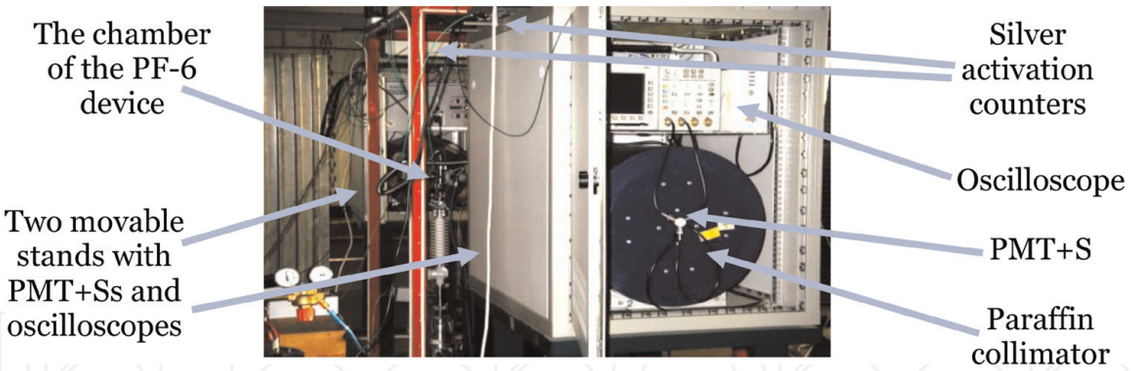


Figure 6.
Experimental complex for measuring the neutrons field produced around the PF-6-based neutron source; it consists of two sets of detectors (silver activation counters and PMT + Ss) placed inside two cabinets.

In **Figure 7**, one may see an oscillogram of a cosmic radiation, demonstrating the temporal resolution of the PMT + S used in the experiments. It appears to be equal to 2.6 ns of its full width at half maximum (FWHM).

In **Figure 8**, the oscilloscope traces (OTs) for low (a), medium (b), and high (c) intensity of hard X-rays and neutrons are presented. It is seen that at a high-intensity of the X-ray and neutron radiations, the photomultipliers are working in a "current mode of operation" (**Figure 8c**) rather than in a "single-pulse" recording (as it is in a and b pictures) regime.

Our plan for the first step of experiments on the taxonomy of a simulator is to investigate the angular characteristics of neutron radiation of the PF-6 device itself in empty room (**Figure 9a**).

It is provided in the most "clean" hall by two stands. In this test, one stand (No. 1) has an immobile position in a direction perpendicular (90°) to the Z-axis of the PF-6 chamber, whereas the other one (stand No. 2) is moved around the PF-6 device.

After these measurements, giving information on the spatial distribution of neutron intensity around the PF-6 device itself, the second step of this procedure starts. In these tests, the same measurements must be done but already with the simulator (in its capacity a chamber of the PF-1000U facility is used). That gives an

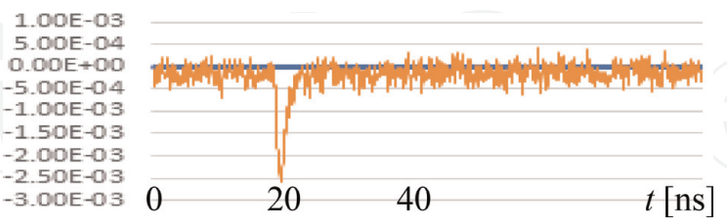


Figure 7.
Oscilloscope trace (OT) of cosmic radiation measured by PMT + S (2.6 ns of its FWHM).

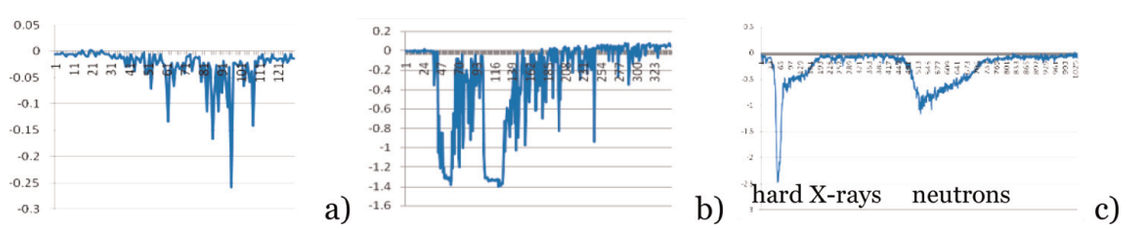


Figure 8.
Oscillograms of three shots with low, medium, and high intensity of hard X-rays (1st pulses) and neutrons (2nd pulses); in the last oscilloscope trace all flashes produced inside the scintillator by individual X-ray photons and neutrons (a, b) are merged (c) and the PMT begins to work in the "current" mode of operation.

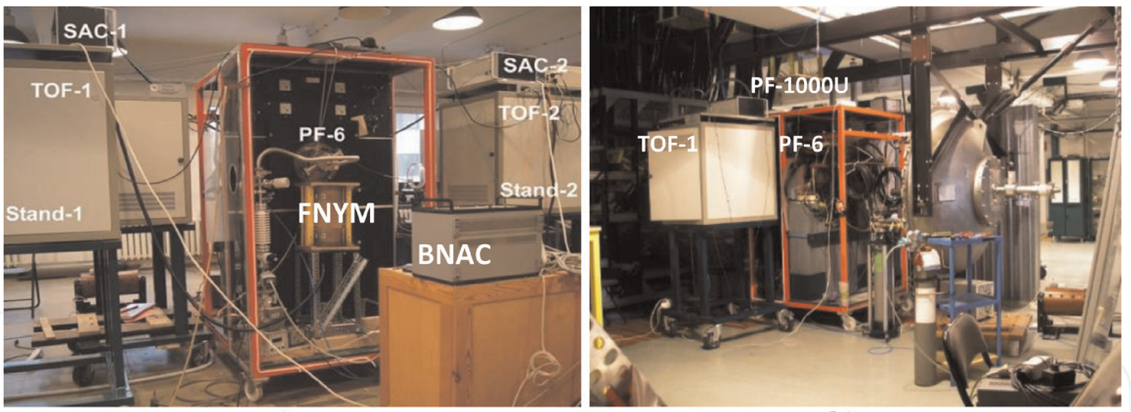


Figure 9.
Steady-state position of the stand No. 1 (SAC-1 and TOF-1) and a movable stand No. 2 (SAC-2 and TOF-2) in its position No. I (see later) in a "clean-room" condition (a) as well as the same stands placed at their 90° positions to the Z-axis of both chambers of PF-6 (neutron source) and PF-1000U (simulator) devices (b).

opportunity to disclosure imperfections produced in the 3-D neutron field by scattering and absorption of 2.5-MeV neutrons in structures of the PF-1000U chamber as well as in the hall parts (**Figure 9b**).

3. Methodology

3.1 Theoretical treatment

3.1.1 Neutron emission anisotropy

The well-known nuclear fusion reaction $D\ (d,n)He^3$ produced by a parallel monoenergetic beam of high-energy deuterons propagating along Z-axis at its interaction with an optically "thin" target (a cloud) of deuterium gas or low temperature deuterium plasma (i.e., when its thickness is much less than the mean free path of deuterons in the cloud) is characterized in the laboratory system of coordinates [20, 21] by the following formula:

$$Q = \frac{4}{3}E_n - \frac{1}{3}E_d - \frac{2\sqrt{2}}{3}\left(E_d \cdot E_n\right)^{1/2} cos\ \theta \tag{2}$$

where Q is the energy released in the reaction, E_d is the energy of a fast deuteron bombarding the deuteron target, E_n is the energy of a neutron, and θ is the angle in relation to Z-axis that neutron is emitted to.

This equation can be resolved, and it gives for neutron energy E_n:

$$\sqrt{E_n} = 0.3535 \cdot \sqrt{E_d} \cdot cos\ \theta \pm \left\{\left(0.125 \cdot\ cos^{\,2}\theta + 0.250\right) \cdot E_d + 2.475\right\}^{1/2} \tag{3}$$

For the angle θ = 90°, this formula takes the simplest form:

$$E_n = \frac{3}{4}Q + \frac{1}{4}\ E_d \tag{4}$$

For the parallel beam of, e.g., 200 and 500-keV deuterons propagating along Z-axis (the angle θ = 0°) and bombarding plasma, the data on neutrons energy that escape the plasma volume (i.e., a target) at some angles are depicted in **Tables 2** and **3**.

Neutrons escaping angle θ_i (°)	Neutrons energy E_n (MeV)
90	2.47
0	3.1
180	2.0

Table 2.
Energy of neutrons produced by 200-keV deuterons with the exit angle θ_i.

Neutrons escaping angle θ_i (°)	Neutrons energy E_n (MeV)
90	2.57
0	3.6
180	1.8

Table 3.
Energy of neutrons produced by 500-keV deuterons with the exit angle θ_i.

Figure 10 represents an angle distribution of the effective differential cross-section σ_{eff} of the reaction $D(d,n)He^3$ in the laboratory system of coordinate. This picture is valid again for the low-intensity parallel monoenergetic beam of deuterons of energy E_d = 500 keV interacting with a "thin" target of deuterium plasma of relatively low temperature [20, 21]. Neutron stream density (fluence) is proportional to the effective differential cross-section σ_{eff}. Now, we can define the neutron anisotropy for the particular plasma device as a ratio of fluencies obtained in different directions:

$$A(\theta_i) = \varphi(\theta_i)/\varphi(90°) \tag{5}$$

where $A(\theta_i)$ is the anisotropy of neutrons emitted at an angle of θ_i to the direction of the beam of fast deuterons (i.e., to Z-axis of a DPF oriented from its anode), $\varphi(\theta_i)$ is the fluence of neutrons emitted at an angle of θ_i, $\varphi(90°)$ is the fluence of neutrons emitted at an angle of 90°, and various i are the subsequent positions where anisotropy is calculated and/or measured. From the next section, one can get that each i denotes the angle that corresponds to the measuring position location.

It gives for the data on anisotropy of neutron streams at various angles normalized to the value at 90° that produced by the beam of 500-keV deuterons at its interaction with a low-temperature deuterium plasma the following values (**Table 4**).

Thus, the theoretical angular distribution of neutron intensity produced in an "optically" thin deuterium gas (or low-temperature plasma) target by a

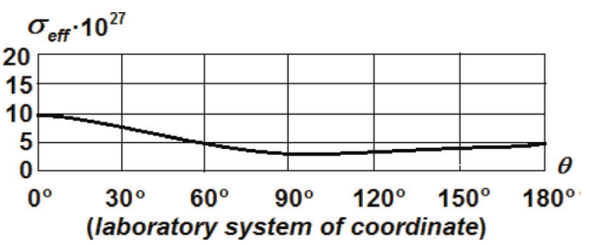


Figure 10.
A graph of the effective differential cross-section σ_{eff} for neutrons taking part in the reaction $D(d,n)He^3$ that is presented for the laboratory system of coordinate in dependence on the angle. The diagram is calculated for the case of the mono-energetic beam of deuterons having energy E_d = 500 keV and interacting with a so-called "thin" target of deuterium plasma of fairly low temperature.

Angle θ_i (°)	Anisotropy coefficient A for the beam of 500-keV deuterons normalized to the value at 90°
90	1.0
0	3.33
180	1.8

Table 4.
Anisotropy coefficient on the exit angle normalized to the value at 90°.

low-intensity parallel mono-energetic beam of 100-keV deuterium ions as test particles (usually for the DPF deuteron spectrum obtained in various conditions, different authors give a figure in the range of hundreds KeV—see e.g., [8, 22]) looks similar to the eight digit (see **Figure 11** plotted for the monoenergetic deuterons of 100-keV energy). In a center-of-mass system, it is symmetrical, whereas in a laboratory coordinate frame, it is slightly shifted in the direction of the beam propagation with $A(\theta_i) \approx 2.0$ and 1.5 for 0 and 180° correspondingly.

However, one has to take into account that the main part of neutrons generated in DPF is produced by gyrating deuterons [8, 22]. These particles escape pinch plasma (target) at a certain effective angle. So, it must give for the direction of Z axis the lower values of anisotropy counted for 100-keV deuterons: $A(\theta_i) \approx 1.7$ and 1.2 for 0 and 180°, respectively.

Moreover, the spectrum of fast deuterons in DPF devices is not monoenergetic: it extends till MeV range following the power law with a peak at hundred keV [8]. As it is known, the deuterons generating neutrons are captured for a certain time by self-produced magnetic fields and then fly out from the pinch under an appreciable angle as it was mentioned above. Besides, this flow of deuterons is very dense and intense (so it may be better characterized as a fast-moving cloud—high-energy and almost relativistic plasma jet) [8, 22].

All these features must result in the obtained experimental data for neutron anisotropy and spectra in smoothing of the pictures compared with the aforementioned theoretical ones. One may expect that the energy of deuterons producing neutrons in a DPF will occupy an energy range in the interval between the above-mentioned values (i.e., for deuterons energy distributions with their peak energy somewhere from 100 till 500 keV).

3.1.2 Time-of-flight spectral measurements

As it is well known [20, 21], the TOF technique converts a temporal behavior of the ns pulse of the neutron emission reflected in the pulse shape for the PMT + S positioned at the close vicinity to the generator into the pulse shape reproducing

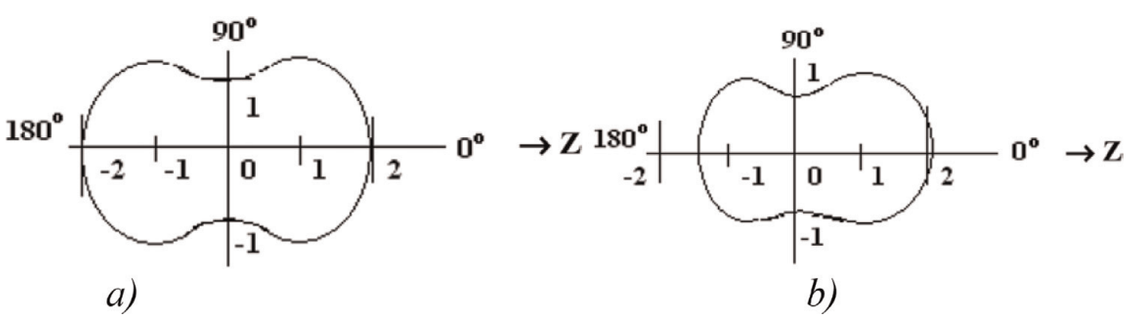


Figure 11.
Theoretical angular distribution of neutron intensity produced in an "optically" thin gas target by a low-intensity parallel monoenergetic beam of 100 keV deuterium ions: in a center-of-mass system (a) and in a laboratory coordinate frame (b).

spectral characteristics of neutron radiation when the fast probes is moved to a certain distance (the speed distribution of particles transfers into the space one).

Time-of-flight of neutrons measured by means of PMT + S can be transformed into the energy distribution of the neutrons producing the neutron pulse. Their maximum may be expressed by a ratio (6) presented in books [20, 21]:

$$E_{MeV} = (72.24\, l_m/t_{ns})^2 \tag{6}$$

In this formula, E_{MeV} is neutron energy in (MeV), l_m is a distance in (m), and t_{ns} is a flying time interval in (ns).

To transform temporal behavior of a neutron pulse in the OT into spectral distribution of neutrons by their energy values in the OT, the distances l from the source till the PMT + S for the observation of spectra must be much longer compared with the size of the neutron pulse in space (in our case $l >> 10$ cm).

3.2 Neutron activation techniques application for the "clean-room" conditions

The first stage of the characterization experiments is the investigation of the angular characteristics of neutron yields of the PF-6 device itself by activation methods. General arrangement of the two stands with SACs and other activation detectors as well as with two stands containing PMT + Ss-related equipment is shown in **Figure 9** in the positions of a "clean-room" condition (a). Note that there is a difference in heights of the positions of PMT + Ss and SACs: the PMT + Ss are situated in the plane of Z-axes of the PF-6 and PF-1000U chambers (that are directed horizontally in relation to the floor) but the SACs are placed 70 cm higher.

This taxonomy of the PF-6 device was provided in the most "clean" hall. However, it must be noted here that these conditions are not absolutely "clean." Indeed, the device itself has four capacitors filled with a castor oil (scatterers), the concrete floor and ceiling are presented, four coils of cables and four separating transformers are the elements of the PF-6 construction. All of these parts are rather bulky scatterers/absorbers. Due to these obstacles, we shall use the term "absolute" neutron yield in the subsequent text for the figures that will represent the values which are only correlate with another instruments' data in the dissimilar positions. Thus, these data are the "virtual" readings, or the "absolute" quantities with the identical but unknown standardizing coefficient.

During the experimental simulations, the neutron yield (Y_{nTOTAL}) is monitored using two SAC(s). The shots of the PF-6 device when the Y_{nTOTAL} magnitude was in the range of 10^8–10^9 neutrons per pulse were taken into account only. Side by side with two silver activation counters (SACs), the activation detectors based on *Be* and *Y* were used. The *Y* neutron detectors give the data that are correlated with the neutron yield obtained from SAC quite well (see **Figure 12**).

The calibration measurements were produced during the successive 33 shots with SAC-1 and SAC-2. These probes were placed normally to the Z-axis of the chamber of the PF-6 device from its two opposite sides. Then keeping the position of the probe with SAC-1, the stand No. 2 was relocated along the way around the PF-6 device with seven different stops shown in **Figure 13**.

The procedure looks as follows. There are two cages. Each cage has a SAC placed 70 cm above the Z-axis of the PF-6 chamber (**Figure 13b**). The Z axis covers the axis of symmetry of the PF device. The X axis is horizontal, so the Y axis is vertical.

For any (x,y,z) point $\theta = arccos\ \{z/\ (x^2 + y^2 + z^2)\}$ is the angle between vector $\left(\vec{x}, \vec{y}, \vec{z}\right)$ and the Z axis. This gives the spatial angles $\theta_i°$ that differ from those

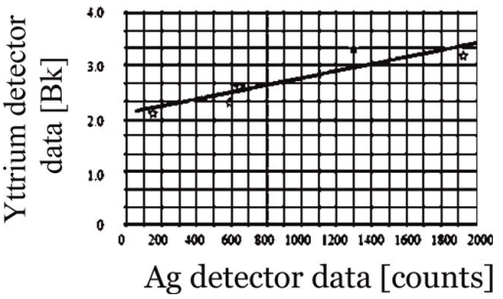


Figure 12.
Data of the absolute neutron yield measured during the experimental session with yttrium and silver activation counters averaged over 10–20 shots for each point of the graph.

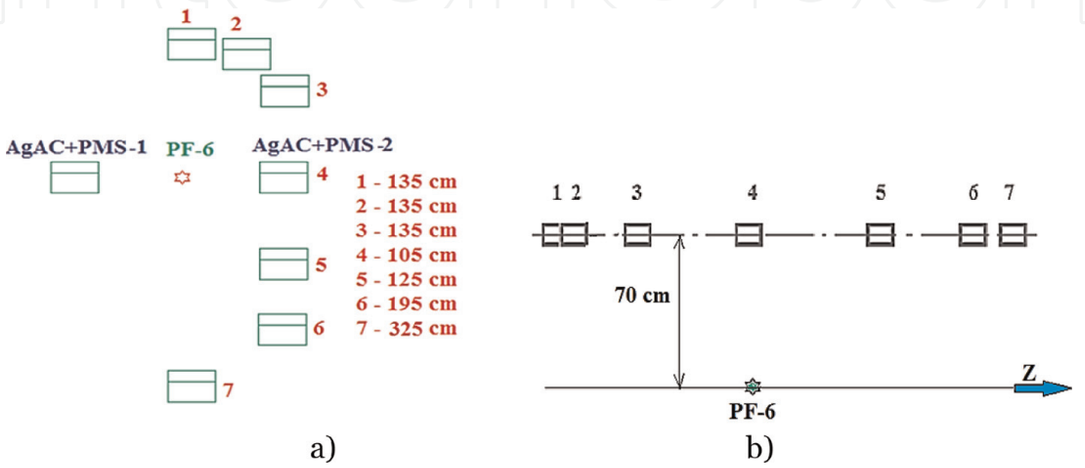


Figure 13.
Presentation of the diagram of the immobile position of the stand No. 1 and seven successive locations of the movable stand No. 2: top view—(a) and side view—(b) during measurements of the angular distribution of "absolute" neutron yield by SACs for the PF-6 device in a "clean" situation.

"flat" angles α_i° depicted in **Figure 13a**. From literature, one may find that neutrons produced in DPF and irradiated in all directions perpendicular to Z-axis (i.e., for the detector SAC-1 in its immobile place and for the detector SAC-2 in the position 4) has usually the energy peak near the value equal to 2.5 MeV for reacting deuteron having energy of hundred' keV [20, 21].

Step 1: At the beginning, the background (i.e., cosmic radiation) data are fixed by both SACs. It is repeated five times and the mean figures (usually it is ~30–40 counts in the case) are computed for each collection of shots.

Step 2: On the assumption that for both SACs placed at 90° (i.e., perpendicular to the Z-axis of the PF-6 chamber—position No. 4 for a movable SAC-2), neutron yields are the same (with this device it was proved many times), and their individual sensitivities ratio is calculated as $Y_{n1}/Y_{n2(position\ 4)} = Q_1$. This is a standardization coefficient Q_1 for all subsequent calculations for different positions of a SAC-2 and for dissimilar neutron outputs in various collections of shots. For example, in this set of experiments, $Q_1 = 1.374$.

Step 3: Data that were collected by the SAC-1 and by the SAC-2 in its different locations ($Y_{n1(i)}$ and $Y_{n2(i)}$) are averaged over about 10–20 "good" shots during a single session, so the mean figures for each collection of shots $Y_{n1(i)measured}$ and $Y_{n2(i)measured}$ are calculated after deducting background values.

Step 4: At that time, the "actual" magnitudes of $Y_{n2(i)}$ of the SAC-2 are calculated with the detector sensitivity correction:

$$Y_{n2(i)real} = Y_{n2(i)measured} \times Q_1 \tag{7}$$

Step 5: The remoteness r_{2i} of the detector SAC-2 from the PF-6 chamber are computed for each of its positions; then a standardization procedure is produced according to the knowledge of the real distance lengths between the source and the SAC-2: $r_{SAC\text{-}2}$. Subsequently by applying the r^{-2} law, the factors for the neutron yield belonging to all locations of the detector SAC-2 are gained:

$$k_i = \left(r_{SAC-2i}/r_{SAC-2(position\ 4)}\right)^{-2} \tag{8}$$

Step 6: By means of the multiplication of the above-mentioned "actual" neutron yields $Y_{n2(i)real}$ with these factors k_i and regularizing them by the character for $Y_{n1(i)}$ in each collection of shots "i," a coefficient of the anisotropy A in the "clean" room is gained finally:

$$A = k_i \left(Y_{n2(i)real}/Y_{n1(i)}\right) \tag{9}$$

3.3 Neutron activation techniques application for the conditions with an object simulating a section of a toroidal chamber of a mainstream fusion facility (the PF-1000U chamber)

Upon obtaining data on the clean-room conditions, the neutron source—PF-6 device—as well as the both fast probes No. 1 (SAC-1 plus TOF-1) and No. 2 (SAC-2 plus TOF-2) must be transported to the simulator, that is, to the PF-1000U facility chamber. In this arrangement, we must repeat the measurements of the same type as above but around the model set representing the tokamak chamber section (**Figure 14**).

The data acquired in this structure (**Figures 14**, **15**, and **9b**) are compared with the previous data (**Figure 9a**) as well as with monitoring of readings of the transportable test desk No. 2 in comparison with the values obtained by the stand No. 1 in its steady-state location.

Besides, in these experiments, a special 2/4-cm stainless steel (SS) supplement (see **Figure 16**) on the top of the PF-6 chamber was mounted that represented an additional irregularity (mainly in forward direction of neutron propagation).

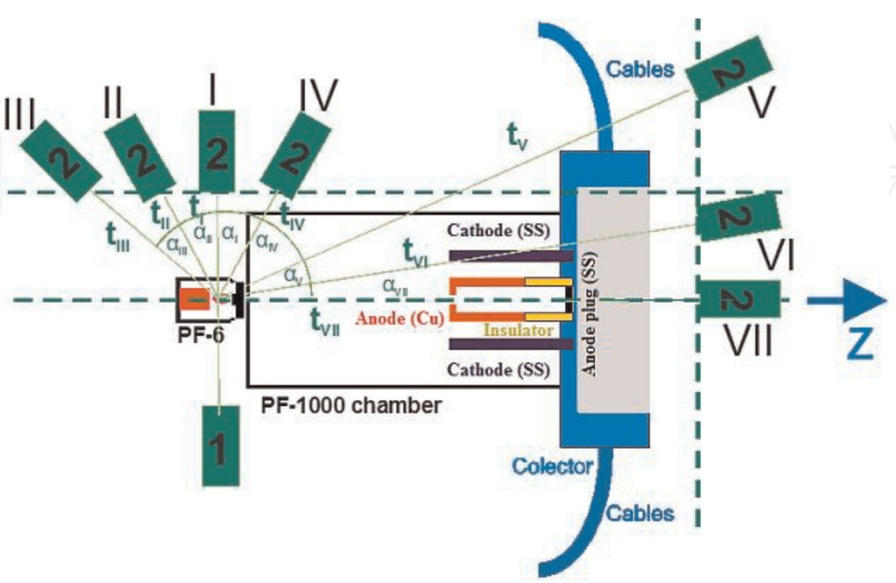


Figure 14.
A scheme of a steady-state location of a stand No. 1 (i.e., the stand containing the activation counter SAC-1 and the fast probe PMT + S—TOF-1) and seven different locations of a movable stand No. 2 during the simulation experiment with the PF-1000U chamber (i.e., a stand with the SAC-2 and the PMT + S probe TOF-2)—top view.

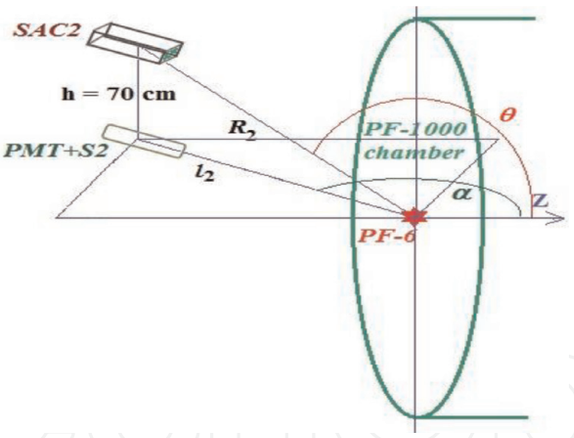


Figure 15.
Distances l_2, R_2 and angles α, θ in the plane of the SACs, and the real 3-D angles from the source to the SAC2, depicted for a hall with a simulator.

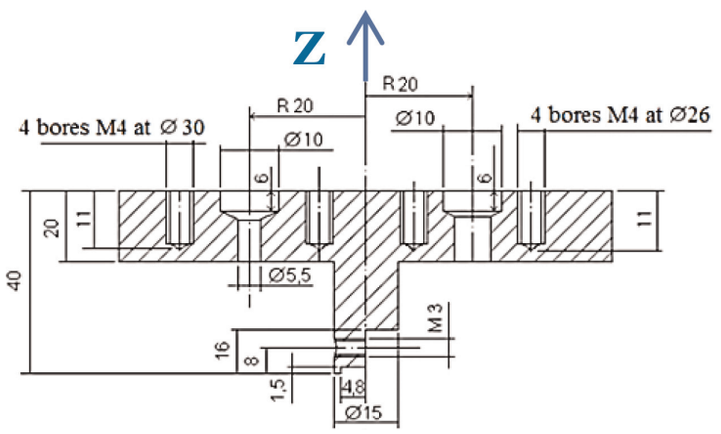


Figure 16.
A stainless steel (SS) supplement placed on the top of the PF-6 chamber in front of the anode; distance between the anode top and the lid's peg was 3.5 cm.

3.4 Neutron spectral measurement procedure by time-of-flight technique for the "clean-room" condition and for the experiments with a simulator

The typical fast probe OT of the PMT + S-1, that is, obtained by the immobile stand No. 1 with TOF-1, for the experiment made in a "clean-room" condition is given in **Figure 17**.

The PMT + S probes No. 1 (immobile) and No. 2 (movable) are placed in the horizontal plane coinciding with a Z-axis of the PF-6 chamber. The above-mentioned TOF method was used to obtain information on the angle neutron spectral distribution. Again, the PMT + S-1 position (TOF-1) was preserved from one side of the PF-6 chamber but the PMT + S-2 stand (TOF-2) was moved along the steps 1 through 7 shown in **Figure 13a**.

As it was mentioned above, the neutrons' energy is 2.5 MeV [8] at the angle 90^0 to Z-axis of the chamber; so for the detectors Nos 1 and 2 placed at 1.05 m we have to move forward the hard X-ray pulse by its time-of-flight equal to 3.5 ns ($v_{hxr} = 3 \times 10^8$ m/s) and the neutron pulse—by 48.5 ns ($v_n = 2.1667 \times 10^7$ m/s) as it is shown in **Figure 18a** and **b**.

This correction on TOF of both types of radiation (we have taken a mean value for it calculated for the 33 shots) provides the time interval for the delay of the neutron pulse peak appeared near the anode of the DPF chamber in relation to the front of the hard X-ray pulse. We found that in these experiments, it was equal to

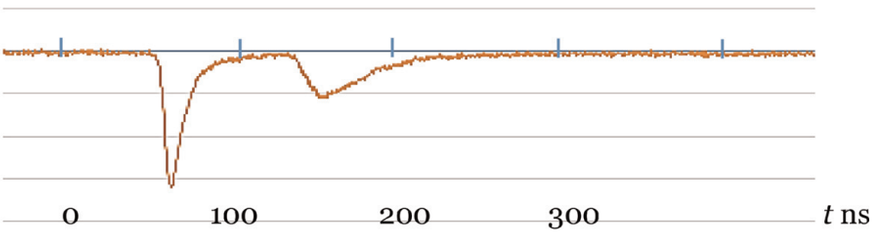


Figure 17.
Typical OT of hard X-ray (1st—Δt_{FWHM} = 10 ns) and neutron (2nd) pulses of the PF-6 device (neutron pulse: Δt_{FWHM} = 20 ns).

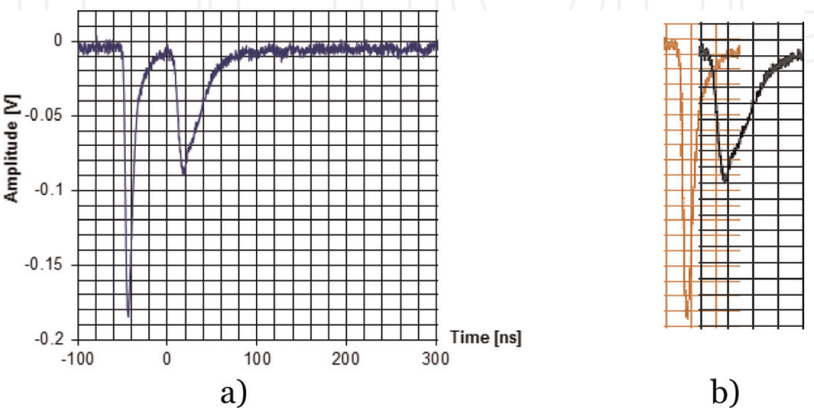


Figure 18.
Initial (measured—a) and corrected for TOF positions of hard X-ray (1st) pulse and 2.45-MeV neutron (2nd) pulse (b).

Δt = 25 ns for each stand in this collection of experiments. Later, one must recheck this figure in each shot by using fixed stand No. 1. Typically, the rise-time of the hard X-ray pulse is vertical practically, that is, it is equal to the fast probe temporal resolution and, consequently, to the measurements' uncertainty. These readings establish for us a foundation for the following measurements and amendments fitted for all other neutron pulses observed at different angles and at dissimilar remoteness from the PF-6-based pulsed source of neutrons. So in every shot, we begin our temporal calculations from the front of the hard X-ray pulses, subsequently moving the neutron pulses to the time moment delayed in relation to the X-ray front namely by this Δt.

After such a procedure, we obtained an opportunity to calculate TOF of this neutron pulse to the detector No. 2 in its each specific location. Using formula (6), this measured and corrected time-of-flight can easily be recalculated into the energy of this neutron group producing the neutron pulse maximum. Results of calculations at usage of the above procedure and the formula give the angle dependence of the neutron spectral distributions in the space around our PF-6 device in a "clean" room conditions.

The same procedure of neutron spectra distortions has been provided in the experiments with the PF-1000U chamber simulator.

4. Numerical simulations

4.1 Geometrical model

We have used a geometrical model of this simulation experiment in a simplified form. The scheme encloses the PF-1000U stainless steel vacuum chamber, a set of

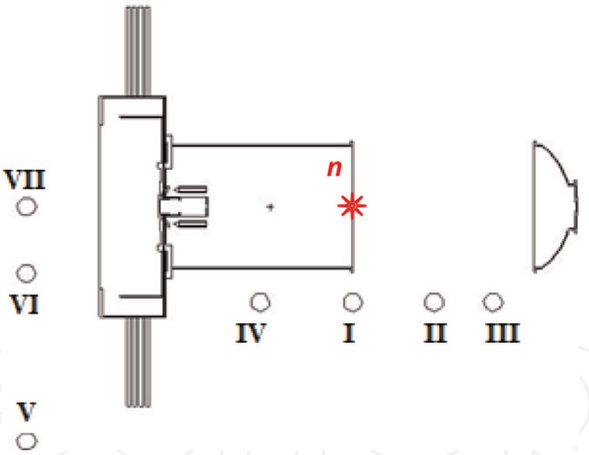


Figure 19.
A cut-view of the geometrical MCNP input: ZX plane. Numbered spheres are "detectors", the star with the letter "n" denotes neutron source (PF-6).

electrodes with insulators, a collector with cables, as well as all details of the hall interior. The vacuum cover of the PF-1000U chamber is detached and removed 2 meters away along Z-axis. Thus, an air is filled in the chamber. A frame of reference is originated in the center of the anode end. The Z-axis is on the axis of symmetry of the chamber, the X-axis is horizontal, whereas the Y-axis is vertical. A cross-section of the model in the X-Z plane is offered in **Figure 14** and in **Figure 19**.

4.2 Neutron source

The source of neutrons is point and lies on the Z-axis near the end of the opened chamber of the PF-1000U facility. The coordinates are (0, 0, 160) cm. The energy spectrum of neutrons is the Gaussian one. The peak of the most probable energy of the Gaussian spectrum of neutrons depends on the direction of neutron emission.

The group of neutrons that are emitted in-Z direction (in opposite direction in the respect to Z-axis) has energy around 2.7 MeV, neutrons that are emitted in XY plane (90° in respect to Z-axis) have their peak energy around 2.45 MeV, and the group of neutrons emanated in +Z direction (i.e., at 0° in respect to Z-axis) has their energy peak around 2.3 MeV. In all in-between directions, the neutron groups have corresponding intermediary energies. The widths of all Gaussian peaks are assumed to be 120 keV. The neutron emissions in all directions are unequal (i.e., anisotropic) as it is described above.

4.3 The code

The MCNP code (X-5 Monte Carlo Team, MCNP—A general Monte Carlo N-particle transport code, Version 5, Los Alamos National Laboratory, LA-UR-03-1987, 2003 [16]) was carried out for calculations. Cross-sections used in these computations have been derived from the ENDF/B-VI library [17].

4.4 Tallies

Calculations of neutron flux density and spectra have been performed for seven spheres of air placed in positions with spherical coordinates that are described in Section 3.2.

Let us denote φ_n (n = I, II, ..., VII) as MCNP calculated neutron flux density in n-th SAC. Then anisotropy $A_n(\theta_n)$ equals:

$$A_n(\theta_n) = \frac{\varphi_n r_n^2}{\varphi_1 r_1^2} \tag{10}$$

Using the above procedure, we have provided test calculations both for neutron anisotropy and spectra for several configurations close to the experimental ones including those for the pulse shape as it is seen in the oscilloscope traces.

5. Results and discussions

5.1 Experimental results on measurements of anisotropy of neutron emission using PF-6 device positioned in an "empty" hall

One may see the results of anisotropy measurements after their processing in **Figure 20**. As in **Figure 13a**, this is the top view. Thus, it is a projection of the plane of SACs (70 cm above Z-axis) to the plane containing PMT + Ss and Z axis. In particular, for example, for the SAC-2, the so-called "flat" angle presented as α = 0° corresponds in the 3-D diagram to the actual angle θ = 12°. Juxtaposition of the experimental figures and the theoretical data (see **Figure 11** and the side analysis) one may find a number of dissimilarities. However as it was mentioned before, the beam of deuterons is not a parallel one because of the magnetization of ions in the self-generated magnetic fields [8, 22]). Besides, this beam of fast deuterons is very powerful and its energy spectrum is very broad extending to the MeV range (so this stream is non-monoenergetic one). It is a reason for the observed in the experiment a certain "leveling" of the "8-digit" form of anisotropy shown in **Figure 11**. In addition, there are two peculiarities of the graph 20 that must be discussed.

1. It is seen that in forward directions (V, VI, and VII), a value of anisotropy is noticeably larger compared with those known from literature [8]. Usually these values are about 1.4–1.7. Such figures can be obtained by means of formula taken from [20, 21] if the most typical deuteron energy will be equal to $E_d \approx 100$ keV and at the condition that the basic part of fusion neutrons are generated by magnetized deuterons that are flying out of the pinch within a cone having an angle to Z axis equal to about 20° [22]. But in these experiments, the magnitudes of neutron fluxes are equal to 1.8, 2.1, and 2.4 observed in these directions.

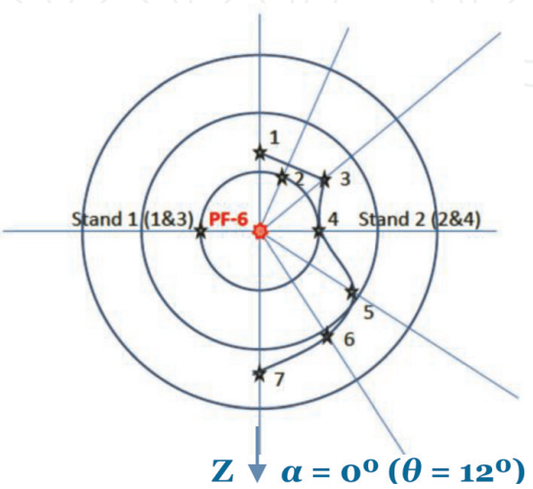


Figure 20.
Polar chart of neutron fluxes measured for different angles in relation to Z-axis of the PF-6 device for the case of the "clean-room" environments (here it is a projection from the plane 70-cm above the plane of Z-axis of the PF-6 chamber); in this chart, the radii of successively enlarged rings correspond to anisotropy coefficients equal to 1, 2, and 3, respectively; the coefficients are normalized on the value for the position 4.

2. One may notice a bit strange result for the position 2 of **Figure 20**: just opposite to the previous case, we observed a low value of the neutron flux measured at the angle α = 157°.

It is possible to find an interpretation of these features by comparing these experimental results with the MCNP modeling of the process.

Some parts of the PF-6 device itself as well as the hall environment can influence the ideal theoretical representation. The Monte-Carlo (MCNP-5) computations have been provided especially to describe the PF-6 itself and its surroundings. As it is known, the MCNP technique does not permit undertaking an inverse problem. Thus, we have provided a number of numerical simulation for the following dissimilar experiment's situations:

1. The source of neutrons placed at the beginning of system of coordinates (in the center of the PF-6 anode surface) is point, isotropic, and monoenergetic (with E_n = 2.5 MeV).

2. Geometry of capacitors, separating transformers, floor, ceiling, and cables is approximate and simplified.

For identification of an influence of each component of the environment, we have provided six successive sets of the computations: with vacuum everywhere and with separating transformers on their places; vacuum everywhere with capacitors in their locations; vacuum everywhere with floor and ceiling of the hall; vacuum everywhere and hank of cables; all components are presented; only vacuum.

3. All calculations of the neutron flux density have been fulfilled for seven detectors placed in their real positions coinciding with those in the present experiments. Detectors were represented by spheres of 15 cm radius each.

Calculations have been done for two cases—with absence and in presence of the cadmium foils enveloping each SAC—see **Tables 5** and **6** correspondingly. The first one contains results of calculations of neutron flux density (cm^{-2}) of the whole spectrum of neutrons reaching the detector. The second one comprises data obtained for calculations of flux density of neutrons with energy spectrum above 500 keV.

The values of flux densities in seven directions around the PF-6 chamber (i.e., anisotropy) were calculated for each case taking into account the distance of the detector from the source using an inverse quadratic law for radii. Examination of these tables shows quite clearly:

1. The cadmium foil enveloping our SACs is a very effective screen preventing penetration to the counter of low-energy neutrons that appears due to multiple scattering in the environment.

2. The first above-mentioned peculiarity of the chart is partially explained by scattering (reflection) of fast neutrons in forward direction on concrete ceiling and floor (for example, at 0° the figure looks as follows: 1.7 × 1.23 = 2.1).

3. The second effect is explained by scattering of neutrons on the coil (bundle) of cables: the data of experiment and modeling coincide numerically almost exactly.

Coordinates and points of neutron flux measurements					PF-6 with separating transformers		PF-6 with capacitors		Hall ceiling and floor		Hanks of cables		All components of the PF-6		Vacuum everywhere	
No	**x**	**y**	**z**	**R**	**MCNP**	**A**	**MCNP**	**A**	**MCNP**	**A**	**MCNP**	**A**	**MCNP**	**A**	**MCNP**	A
1	0	58	−135	146.932	3.92E-06	**1.04**	3.93E-06	**1.02**	5.10E-06	**1.08**	3.77E-06	**1.02**	5.27E-06	**1.09**	3.70E-06	**1.00**
2	54	58	−127	149.6964	3.69E-06	**1.01**	3.79E-06	**1.02**	4.95E-06	**1.09**	2.91E-06	**0.81**	4.31E-06	**0.92**	3.56E-06	**1.00**
3	105	58	−85	147.017	3.85E-06	**1.02**	3.89E-06	**1.01**	5.10E-06	**1.08**	3.77E-06	**1.02**	5.23E-06	**1.08**	3.71E-06	**1.00**
4	105	58	0	119.9542	5.68E-06	**1.00**	5.77E-06	**1.00**	7.07E-06	**1.00**	5.57E-06	**1.00**	7.28E-06	**1.00**	5.55E-06	**1.00**
5	105	58	68	137.8876	4.28E-06	**1.00**	4.40E-06	**1.01**	5.64E-06	**1.05**	4.20E-06	**1.00**	5.84E-06	**1.06**	4.20E-06	**1.00**
6	105	58	164	203.1871	1.97E-06	**1.00**	2.05E-06	**1.02**	3.08E-06	**1.25**	1.93E-06	**1.00**	3.22E-06	**1.27**	1.93E-06	**1.00**
7	0	58	325	330.1348	7.45E-07	**0.99**	7.84E-07	**1.03**	1.36E-06	**1.46**	7.33E-07	**1.00**	1.43E-06	**1.49**	7.37E-07	**1.01**

Table 5.
Results of calculations of neutron flux density (cm^{-2}) of the whole spectrum of neutrons reaching the detector.

Taxonomy of Big Nuclear Fusion Chambers Provided by Means of Nanosecond Neutron Pulses
DOI: http://dx.doi.org/10.5772/intechopen.89364

Coordinates and points of neutron flux measurements					PF-6 with separating transformers		PF-6 with capacitors		Hall ceiling and floor		Hanks of cables		All components of the PF-6	
No	**x**	**y**	**z**	**R**	**MCNP**	**A**	**MCNP**	**A**	**MCNP**	**A**	**MCNP**	**A**	**MCNP**	**A**
1	0	58	−135	146.932	3.91E-06	**1.03**	3.77E-06	**1.00**	4.26E-06	**1.04**	3.75E-06	**1.01**	4.40E-06	**1.06**
2	54	58	−127	149.6964	3.69E-06	**1.01**	3.63E-06	**1.00**	4.12E-06	**1.04**	2.90E-06	**0.81**	3.46E-06	**0.86**
3	105	58	−85	147.017	3.84E-06	**1.02**	3.77E-06	**1.00**	4.26E-06	**1.04**	3.76E-06	**1.02**	4.37E-06	**1.05**
4	105	58	0	119.9542	5.67E-06	**1.00**	5.64E-06	**1.00**	6.17E-06	**1.00**	5.55E-06	**1.00**	6.25E-06	**1.00**
5	105	58	68	137.8876	4.28E-06	**1.00**	4.28E-06	**1.00**	4.78E-06	**1.02**	4.20E-06	**1.00**	4.84E-06	**1.02**
6	105	58	164	203.1871	1.97E-06	**1.00**	1.98E-06	**1.01**	2.39E-06	**1.11**	1.93E-06	**1.00**	2.42E-06	**1.11**
7	0	58	325	330.1348	7.45E-07	**0.99**	7.50E-07	**1.01**	9.98E-07	**1.23**	7.33E-07	**1.00**	1.01E-06	**1.22**

Table 6.
Results of calculations of neutron flux density [cm^{-2}] of the spectrum of neutrons above 0.5 MeV reaching the detector.

Examination of our geometry of the PF-6 chamber used in these experiments has also shown that too high intensity in the "forward" direction (points 5, 6, and 7—values up to 2.4) may be explained (additionally to the above-mentioned influence of concrete ceiling and floor) very likely by a specificity of the anode construction in this case. Instead of an aperture usually made in the anode center to prevent evaporation of debris by the electron beam we had in this case a special central insert made of rhenium. In this case, such an insert made of refractory materials helps to produce the most representative group of fast deuterons having higher energy compared with a common case. We observed some years ago this effect with the central anode insert made of tungsten. Because of this fact, the value of the projection of $E_{d\ max}$ onto Z axis appears to be here in the range 150–200 keV, whereas the real value of these deuterons taking into consideration their preferential escaping angle [22] of about 25° can be estimated approximately as 300 keV.

5.2 Data on anisotropy measurements of neutron emission using PF-6 device in the presence of the simulator of a section of a toroidal chamber of a mainstream fusion facility (the PF-1000U chamber)

The process of measurements of neutron fluxes in different directions is about the same as above for the case of the empty hall with a bit different distances from the neutron source to the Faraday cages No. 1 and No. 2 (they were recalculated). Results of these measurements and their treatment including construction of an anisotropy graph are depicted in **Table 7** (together with the "clean-room" data for comparison) and in **Figure 21** presented here for demonstrativeness. This picture is a polar chart analogous to that of **Figure 20**. It presents quite perceptibly both data on anisotropy obtained in a "clean" room conditions (shown by green color) and in a hall with a simulator of a tokamak chamber section (red color). This large-scale object is represented here by a discharge chamber of the PF-1000U installation (see **Figure 14**). In particular, one may clearly see a strong influence of the PF-6 chamber supplement (**Figure 16**) and PF-1000U chamber electrodes (**Figure 14**) produced upon the neutron flux densities under the measurements. Indeed, it becomes apparent in the position V: here between the SAC-2 and the source, the flat part of the supplement (2 cm of stainless steel) is situated; it is even more evident for the locations VI and VII where the SAC-2 records the neutron flux passing through the supplement's protrusion (here we have 4 cm of SS) and through the PF-1000U chamber electrodes. At the same time, just contrary—in the locations of the SAC-2 numbers III, II, I, and IV, the data obtained in this experiment feebly differ from the readings attained in the empty room (positions 1, 2, 3, 4, 5 of the SAC-2).

For the position III, which is close to the location 2 in the empty-room conditions, the same peculiarity (a small dip) in the neutron flux density is observed. It is a consequence of the presence of the same object as in the above-presented

Positions of the detectors SAC&PMT + S2 during the tests with the simulator	III	II	I	IV	V	VI	VII
A—an anisotropy coefficient in the simulation tests	1.17	1.31	1.0	2.16	1.63	0.415	0.13
Positions of the SAC&PMT + S2 during the "clean-room" framework tests	1	2	3	4	5	6	7
A—an anisotropy coefficient in the "clean-room" framework tests	1.3	1.0	1.4	1.0	1.8	2.1	2.4

Table 7.
Data on anisotropy of the neutron yield in the hall with the simulator.

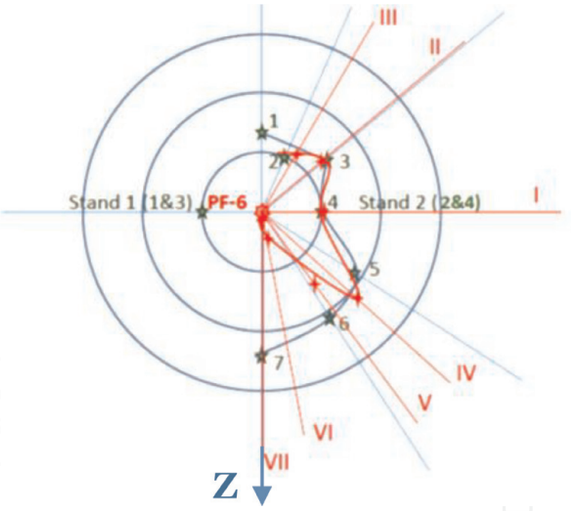


Figure 21.
Polar diagram of neutron yield measured for the PF-6 device in the conditions with a simulator of a section of a tokamak chamber by means of the discharge chamber of the PF-1000U facility; it is shown by red color (the green color diagram refers to the "empty-room" condition).

"clean-room" conditions (an influence upon the neutron radiation produced by the cables bundle). A noticeable influence of the PF-1000U chamber may be seen in the location V (in this very direction the scatterers/absorbers obstacles are cables of the PF-1000U facility—see **Figure 14**). In the locations VI and VII where the SAC-2 is blocked by a thick SS supplement of the PF-6 chamber itself and by the central part of the chamber of PF-1000U device (electrodes), the SAC-2 readings were dramatically decreased.

This chart is again an image projection of a polar diagram presenting both data on anisotropy obtained in a "clean" room conditions (shown by green color) and with a simulator (red color) in the plane of SACs that are 70 cm higher than the level with Z axes of PF-6 and PF-1000U facilities and the detectors PMT + Ss. This is a vertical projection of the neutron flux angular distribution to the horizontal plane containing Z axes of both devices as it is shown in **Figures 13** and **14**. After this session, we came to processing of data obtained with fast probes (PMT + Ss).

5.3 Experimental results on measurements of spectra of neutron emission using PF-6 device with an object simulating a section of a toroidal chamber of a mainstream fusion facility (the PF-1000U chamber)

First, we made the measurements in the "clean room" condition. We preserved the PMT + S-2 position from one side of the DPF chamber (at 105 cm) but moved PMT + S-4 along the steps shown in **Figure 14**. In the direction perpendicular to Z-axis (at the angle 90^0) of the chamber as it was mentioned above the neutrons' energy is 2.5 MeV [1]. Thus to tie the neutron pulse to the X-ray pulse in the center of the PF-6 chamber for the detectors Nos 1 and 2 placed at 1.05 m, one have to shift forward in time the hard X-ray pulse by 3.5 ns ($v_{hxr} = 3 \times 10^8$ m/s) and the neutron pulse by 48.5 ns ($v_n = 2.1667 \times 10^7$ m/s) in a way that is presented in **Figure 18a** and **b**. As a result of this process (averaged over 33 shots), the delay time of neutron pulse maximum inside the chamber in relation to the hard X-ray pulse front has been found as $\Delta t = 25$ ns for both stands. In this set of experiments and later we checked this figure in each shot by using fixed stand No. 1. After these experiments, we obtained the basic data for the subsequent measurements and corrections that have to be done for all other neutron pulses registered at different angles and at dissimilar distances from the neutron source based on the PF-6 device.

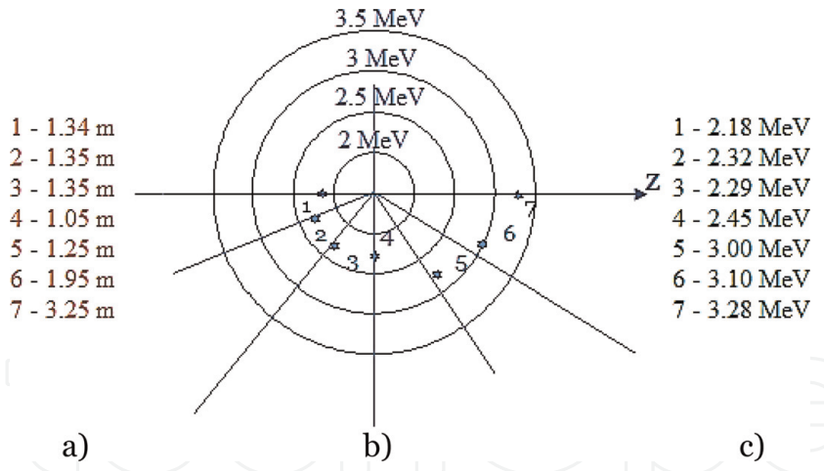


Figure 22.
Angular tracking of energy distribution of neutrons at the PF-6 device in "clean" conditions: (a)—distances from the source (PF-6) to the detector (PMT + S No. 2); (b)—polar diagram of the angular tracking of neutron energy distribution; (c)—data table of energies measured in the specific points.

Each time we begin from the front of the hard X-ray pulse, moving neutron pulse to the point delayed to the front by Δt inside the chamber. Then the TOF of this neutron pulse from the chamber to the detector No. 2 in each specific location is calculated. This time-of-flight can easily be recalculated into the energy of this neutron group by formula (6). Results of calculations gave us the angle tracking of the neutron spectral distribution in the space around our PF-6 device in a "clean" room that is presented in **Figure 22**.

In the next step, we have compared these results obtained by PMT + Ss with the data attained with the PF-1000U discharge chamber (**Figure 14**). The procedure looks as it was before for the "clean-room" experiment.

Again in the beginning, we made measurements of the delay of the maximum of a neutron pulse in relation to the front of the pulse of hard X-rays inside the DPF chamber. For the fixed stand No. 1 placed now at a distance of 0.9 m from the source the delay time of hard X-ray pulse here was 3 ns. The neutron pulse maximum inside the chamber in relation to the hard X-ray pulse front was found now to be in the interval of 9...18 ns in different sets of shots—see e.g., **Figure 23**.

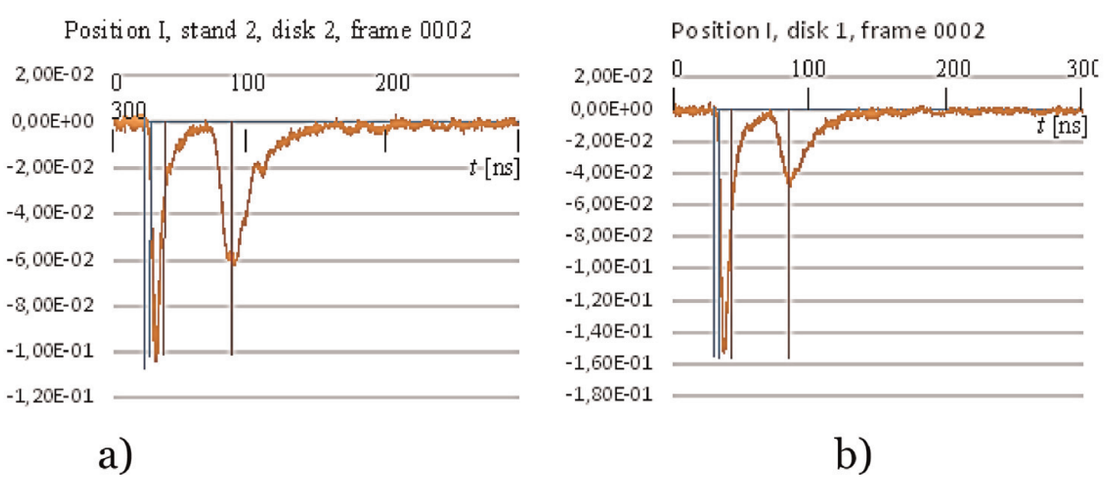


Figure 23.
OTs obtained at 1.1-m distance from the source by a movable stand No. 2 (a) at the location perpendicular to Z-axis (position I of 14) and by a fixed stand No.1 placed at the distance of 0.9 m (b)—both with vertical lines showing shifts of the fronts of the hard X-ray pulses (first, blue) and of the maxima of the neutron pulses (second, red) by their time-of-flights for 2.5-MeV neutrons.

Positions of the PMT + S No. 2 in the simulation experiments	III	II	I	IV	V	VI	VII
Distances l [m] in a horizontal plane from the source to the PMT + S No. 2	1.9	1.42	1.1	1.5	4.5	3.655	3.6
Observation angles $\theta°$ to the PMT + S No. 2 from the neutron source	150°	129°48′	90°	47°10′	37°	11°30′	0°
Energy of the maxima of the first peak of neutron pulses measured in the simulation experiment (MeV)	2.08	2.21	2.45	2.83	2.99	3.28	3.07

Table 8.
Data on the angular tracking of energy distribution of neutrons at the PF-6 device in the hall with a simulator of a tokamak section (the PF-1000U discharge chamber) with angles and distances in a horizontal plane with Z-axis of both devices and PMT + Ss.

The values calculated from the OTs for the simulation experiment are shown in **Table 8** and in a polar diagram (**Figure 24**) where the "clean-room" conditions are depicted by blue color (a lower half-plane) and the simulator experimental data are presented by the red one (the upper half-plane).

The circles in this polar diagram have the same meanings as above: 2.0, 2.5, 3.0, and 3.5 MeV outwards.

From this diagram and the table, one may see that the difference in energy values between "clean-room" conditions and simulation experiments observed almost at all angles is not very much. The real change may be seen in forward direction along Z-axis. It is not surprising—namely in this zone, we have the most serious obstacles in the PF-6 and in the PF-1000U chambers (the stainless steel supplement of the PF-6 device, electrodes of the PF-1000U facility, and several metallic disks for vacuum preservation) that can lead to multiple scattering of even high-energy neutrons. But these features are not the only ones. Some other OTs demonstrate facts connected with the movable stand No. 2 when it is placed in large distances from the PF-6 device and at angles below 90°. In these positions (IV, V, VI, and VII), PMT + S-4 registered hard X-ray and neutron pulses passed through the PF-1000U chamber and interacting with its material. Among them:

- Amplitudes of the pulses became lower by more than 100 times than at 1 m.
- Multiple peaks are observed in the OTs of the movable stand beside the main peaks of hard X-rays and neutrons.
- Extended tail of the neutron pulse has additional peaks.

The first detail cannot be explained by the larger distance only: the quadratic law results in only an order of magnitude lower value [e.g., $(l_V = 4.5\ \text{m}/l_I = 1.1\ \text{m})^2$], that is, it gives merely a coefficient about 16. It means that we have in reality a strong absorption and scattering of hard X-rays and neutrons by our simulator.

The second characteristic gives a certain difficulty in interpretation. It appears that the first set of pulses following the main hard X-ray pulse cannot be attributed to the neutron ones because their energy calculated on the TOF bases gives a value much higher compared with the initial ones (above 10 MeV). Examination with high magnification of hard X-ray pulse shapes of the low intensity obtained at small distances by the probe No. 1 has shown that they have the same multiple peaks as in the probe No. 2 at large distances. Moreover, it appears that these subsequent pulses contain higher energy X-ray photons compared with the first pulse. We observe already in our earlier experiments such a phenomenon (see e.g., [23, 24]). Because

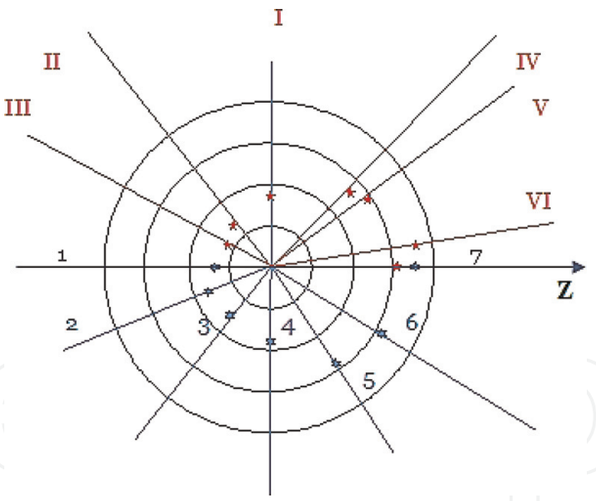


Figure 24.
A polar diagram showing angular energy distribution around a simulator (upper hemisphere, red) versus the angular tracking of neutron energy distribution in the "clean-room" conditions (lower hemisphere, blue).

of the higher energy of photons, a penetrability of each subsequent pulse appeared to be greater than the previous ones. That is why these pulses are sounder in these OTs. Their origin is the multiple current disruptions after the main one taking place during the DPF operation.

Multiple peaks and a very long "tail" of the neutron pulse is explained by neutron reflections and scattering on various elements of the PF-1000U chamber and its auxiliary equipment. We were able to attribute one neutron pulse (a quite high peak) to a real object-scatterer in the OT of the probe No. 2 at its VI position. It appears that the scatterer is a high-pressure cylinder with deuterium (10 liters, 150 atm) placed close to the PF-6 device.

6. Conclusions

1. The analysis provided above has demonstrated that the powerful nanosecond neutron pulses generated by a dense plasma focus device open very promising perspectives in taxonomy of the large main-stream nuclear fusion reactor's chamber. Such extremely bright neutron flashes allow using simultaneously two neutron measurements methodologies—a number of activation techniques and a time-of-flight method—that are able to characterize big chambers of nuclear fusion reactors as neutron scatterers and absorbers. They can fix the most important elements distorting the main characteristics of 3-D neutron fields around them—anisotropy of neutron flux densities and neutrons spectra.

2. Measurements of absolute neutron yield and spectra in seven directions around the neutron source (i.e., the anisotropy of the yield) based on the PF-6 device in the most "clean" (with a minimum of scatterers and absorbers of neutrons) environment has been fulfilled successfully for characterization of the source itself.

3. Subsequent measurements of neutron flux densities and spectra in seven directions around the neutron source based on the PF-6 device in the presence of a simulator of a section of a main-stream fusion facility of the tokamak type (i.e., anisotropy of the yield) have been provided.

4. MCNP calculations with and without a simulator of a section of the mainstream fusion facility have been executed to fix the most important scatterers and absorbers in the experiment.

5. It was found by these modeling, what are the types of influences produced by the environment in both cases on the absolute neutron yield, its angular distributions, and the angle tracking of neutron spectral mapping.

6. Absolute neutron yield calculated over the whole spectrum of neutrons for the detectors in all directions is higher compared with the "vacuum" case by about 10–20% due to multiple scattering of neutrons in the PF-1000U chamber and its environment.

7. The distortions inserted by multiple neutron scattering become important in a very low energy "tail" of the oscilloscope traces and they cannot be observed by PMT + S probes. So, we have to use neutron activation counters to fix these features constructing the anisotropy of the neutron yield.

8. Just opposite to the above-mentioned case, a decrease of the number of fast neutrons due to absorption/scattering can be detected namely by the fast probes technique.

Acknowledgements

This research was provided partially in the frame of the R.F. state task No. 075-00746-19-00 and was supported by the International Atomic Energy Agency (grants IAEA CRP nos. 17167, 19248, 19253, 22745 and 23664).

Author details

Vladimir Gribkov[1,2*], Barbara Bienkowska[1,2], Slawomir Jednorog[3], Marian Paduch[3] and Krzysztof Tomaszewski[4]

1 Interreginal Public Institution Moscow Physical Society, Moscow, Russia

2 A.A. Baikov Institute of Metallurgy and Material Science, Moscow, Russia

3 Institute of Plasma Physics and Laser Microfusion, Warsaw, Poland

4 ACS Ltd., Warsaw, Poland

*Address all correspondence to: gribkovv@rambler.ru

IntechOpen

© 2019 The Author(s). Licensee IntechOpen. This chapter is distributed under the terms of the Creative Commons Attribution License (http://creativecommons.org/licenses/by/3.0), which permits unrestricted use, distribution, and reproduction in any medium, provided the original work is properly cited. CC BY

References

[1] Gribkov VA, Bienkowska B, Paduch M. Examination of a chamber of a large fusion facility by means of neutron activation technique with nanosecond neutron pulse generated by dense plasma focus device PF-6. Fusion Engineering and Design. 2018;**125**: 109-117. DOI: 10.1016/j.fusengdes.2017.10.023

[2] Available from: http://www.ccfe.ac.uk/jet.aspx

[3] Available from: http://www.ipp.mpg.de/16900/w7x

[4] Available from: https://www.iter.org/

[5] Available from: https://www.vniief.ru and https://lasers.llnl.gov/

[6] Available from: http://www.sandia.gov/z-machine/

[7] Stygar W, Austin K, Awe T, Bailey J, et al. Conceptual design of a 960-TW accelerator powered by impedance-matched Marx generators. In: Proc. of the IEEE 21st International Conference on Pulsed Power (PPC); 18-22 June 2017; Brightone East Sussex, United Kingdom. Available from: https://ieeexplore.ieee.org/document/8291256/

[8] Bernard A, Bruzzone H, Choi P, Chuaqui E, et al. Scientific status of dense plasma focus researches. Journal of the Moscow Physical Society. 1998;**8**: 93-170

[9] Scholz M, Miklaszewski R, Gribkov VA, Mezzetti F. PF-1000 device. Nukleonika. 2000;**45**(3):155-158

[10] Scholz M, Bienkowska B, Gribkov VA. Dense plasma focus for applications in positron emission tomography, Czechoslovak. Journal of Physics. 2002;**52**(Supplement D): D85-D92

[11] Gribkov VA, Karpinski L, Strzyzewski P, Scholz M, Dubrovsky AV. New efficient low-energy dense plasma focus in IPPLM. Czechoslovak Journal of Physics. 2004; **54**(Suppl C):C191-C197

[12] Gribkov VA, Dubrovsky AV, Scholz M, Jednorog S, et al. PF-6—an effective plasma focus as a source of ionizing radiation and plasma streams for application in material technology, biology and medicine. Nukleonika. 2006;**51**(1):55-62

[13] Yurkov DI, Dulatov AK, Lemeshko BD, Golikov AV, et al. Pulsed neutron generators based on the sealed chambers of plasma focus design with D and DT fillings. Journal of Physics: Conference Series. 2015;**653**:012019. DOI: 10.1088/1742-6596/653/1/012019

[14] Jednorog S, Szydlowski A, Bienkowska B, Prokopowicz R. The application of selected radionuclides for monitoring of the D–D reactions produced by dense plasma-focus device. Journal of Radioanalytical and Nuclear Chemistry. 2014;**301**(1):23-31

[15] Tilley DR, Cheves CM, Godwin JL, et al. Energy levels of light nuclei a = 5, 6, 7. Nuclear Physics A. 2002;**708**:3-163

[16] MCNP—A general Monte Carlo N—Particle Transport Code, Version 5, X-5 Monte Carlo Team LANL; 2003

[17] MCNP5DATA: Standard Neutron Photoatomic, Photonuclear, and Electron Data Libraries for MCNP5 (CCC-710). Vol I. Available from: http://www-xdiv.lanl.gov/projects/data/nuclear/mcnpdata.html

[18] Bienkowska B, Prokopowicz R, Scholz M, Kaczmarczyk J, Igielski A, Karpinski L, et al. Neutron counter based on beryllium activation. In: AIP

Conference Proceedings 1612. 2014. pp. 105-108. DOI: 10.1063/1.4894033

[19] Available from: http://www.acs-tm.pl

[20] Curtiss LE. Introduction to Neutron Physics. Princeton, NJ: Van Nostrand; 1959. p. 380

[21] Vlasov NA. Neutrons (*Neitrony*), M: Nauka. 1971. p. 551 (in Russian)

[22] Gribkov VA, Banaszak A, Bienkowska B, Dubrovsky AV, Ivanova-Stanik I, Jakubowski L, et al. Plasma dynamics in PF-1000 device under the full-scale energy storage: II. Fast electrons and ions characteristics versus neutron emission parameters, and the gun optimization properties. Journal of Physics D: Applied Physics. 2007;**40**: 3592-3607

[23] Gribkov VA, Miklaszewski RA, Chernyshova M, Scholz M, et al. A single-shot nanosecond neutron pulsed technique for the detection of fissile materials. Journal of Instrumentation. 2012;**7**:C07005. DOI: 10.1088/1748-0221/7/07/C07005

[24] Gribkov VA. The "FLORA" facility (DPF of Filippov geometry of electrodes with pulsed laser on neodymium glass) for investigations of dense magnetized plasma and combined interaction with it of powerful laser light and streams of charged particles. In: Encyclopedia of Low Temperature Plasma. Fortov VE, Series B, editors. Vol. IX-3: Radiation plasma-dynamics": Moscow, Yanus-K, pp. 40-130 (in Russian)